Supporting Information

Mechanochemistry-induced Recycling of Spent Lithium-ion Batteries for Synergistic Treatment of Mixed Cathode Powders

Youzhou Jiang[a], Xiangping Chen[b]*, Shuxuan Yan[a], Yudie Ou[a] and Tao Zhou[a]*

[a] Hunan Provincial Key Laboratory of Chemical Power Sources, College of Chemistry and Chemical Engineering, Central South University, Changsha 410083, P.R. China;

[b] School of Environmental Science and Engineering, Shaanxi University of Science & Technology, Xi'an 710021, P.R. China.

*Corresponding authors:

chenxiangping@sust.edu.cn (X-P. Chen); zhoutao@csu.edu.cn (T. Zhou).

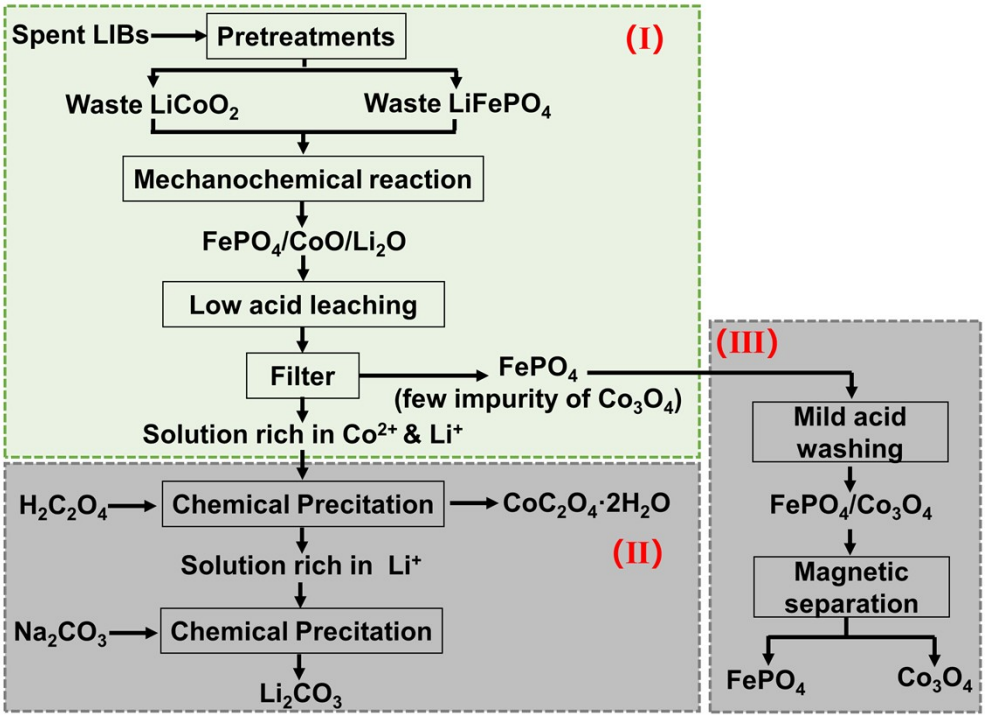

Fig. S1. The proposed green approach for synergetic recovery different cathodes materials from spent LIBs though mechanochemical process. Part (I): Experimental process of mechanochemical reaction and stoichiometric acid leaching for recovering different cathodes from spent LIBs, in which pretreatments include discharge, dismantling, and detachment; Part (II): Separation and recovery of cobalt and lithium compound products; Part (III): Purification and recovery of $FePO_4$.

Note: During pretreatment process, $LiPF_6$ in electrolytes will be quickly decomposed into solid LiF and gaseous PF_5 with the detailed chemical reaction of $LiPF_6(l) \rightarrow LiF(s) + PF_5(g)$. The gaseous PF_5 can be absorbed by specific adsorbents and the solid LiF will usually flow into the slag due to its high melting point (848^{o}C) and boiling point (1681^{o}C). And the composition of leaching residues after leaching of mixed cathode materials is mixture of $FePO_4$, little amount of Co_3O_4 impurity.

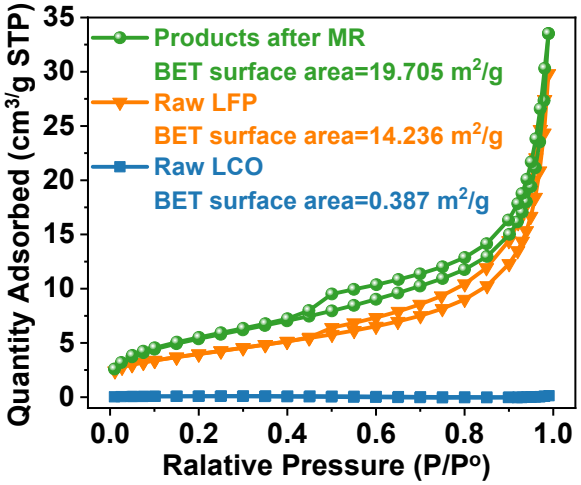

Fig. S2. Nitrogen adsorption-desorption curves of raw materials and product after mechanochemical reaction (conditions: molar ratio of LCO:LFP = 1:1, rotation speed- 650 rpm, mechanical milling time- 5 h, mass ratio of ball to powder- 50:1).

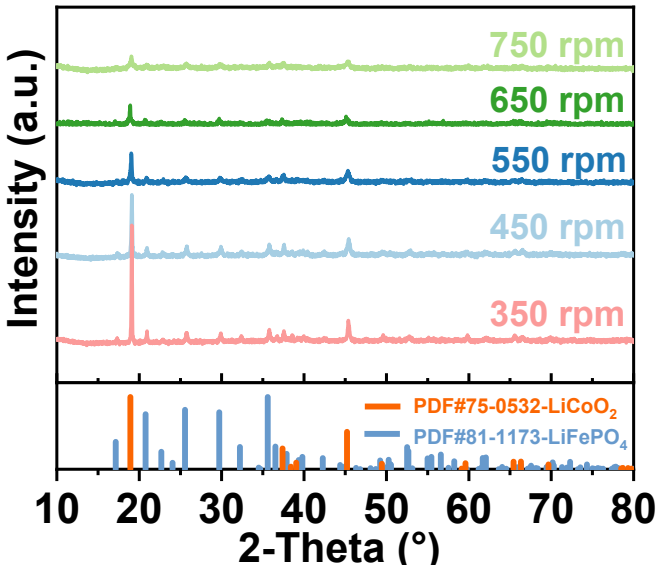

Fig. S3. XRD patterns of samples under different rotation speed. (conditions: molar ratio of LCO:LFP = 1:1, mechanical milling time- 5 h, mass ratio of ball to powder- 50:1)

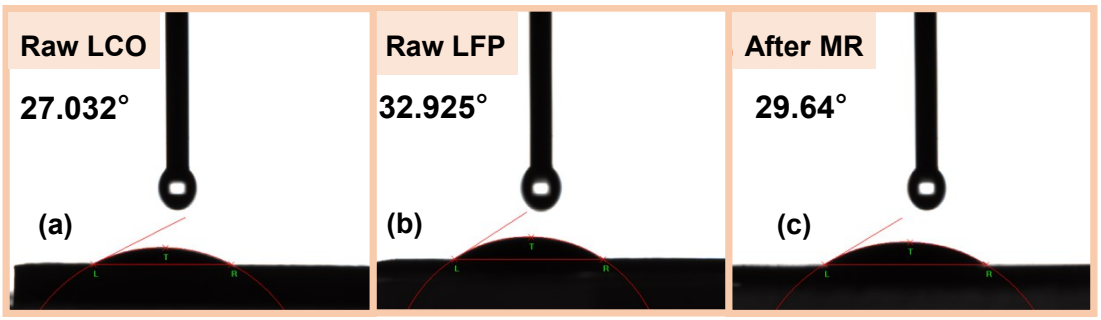

Fig. S4. Contact angle of water on the surface of (a) raw LCO, (b) raw LFP and (c). samples after mechanochemical reaction (conditions: molar ratio of LCO:LFP = 1:1, rotation speed- 650 rpm, mechanical milling time- 5 h, mass ratio of ball to powder- 50:1).

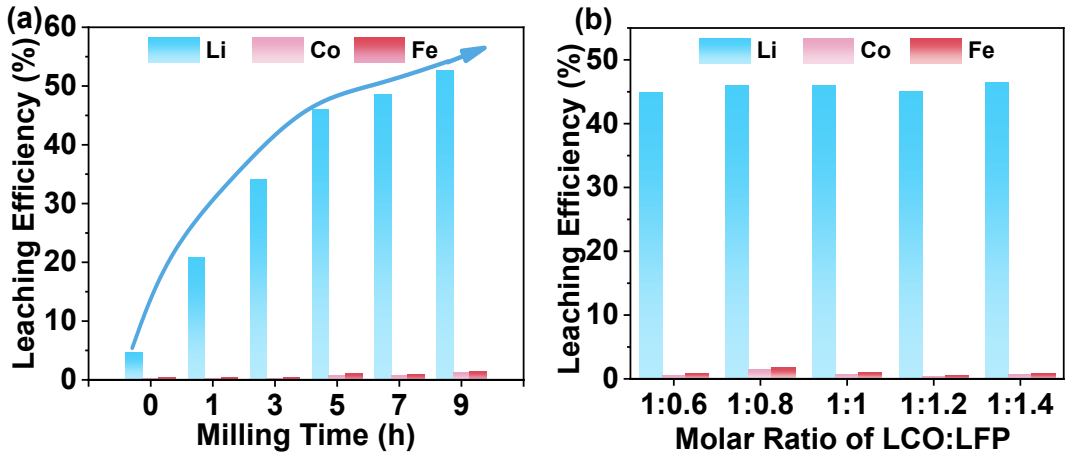

Fig. S5. Effect of (a) milling time and (b) molar ratio of LCO:LFP on the leaching efficiency of metal elements by water leaching.

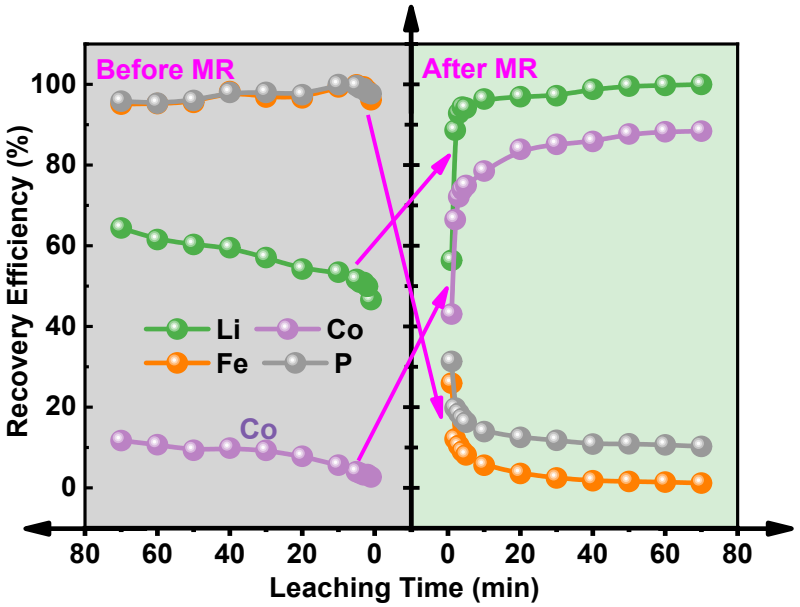

Fig. S6. Illustration of different leaching behaviors for different elements before and after MR. (650 rpm, 5 h, LCO: LFP=1:1, ball to powder ratio of 50:1; 0.15M H_2SO_4).

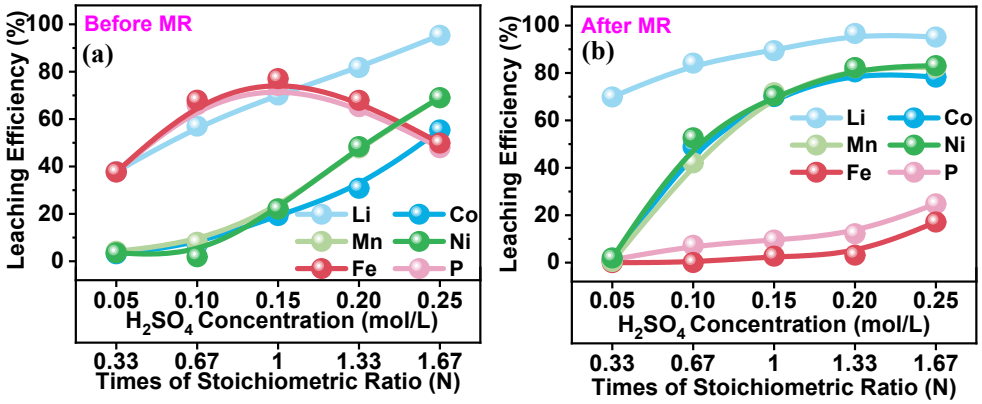

Fig. S7. The leaching behaviors for samples ($LiFePO_4$ and $LiNi_{0.5}Co_{0.2}Mn_{0.3}O_2$) with different acid concentrations before (a) and after (b) mechanochemical reaction. (conditions: molar ratio of NCM:LFP = 1:1, rotation speed- 650 rpm, mechanical milling time- 5 h, mass ratio of ball to powder- 50:1).

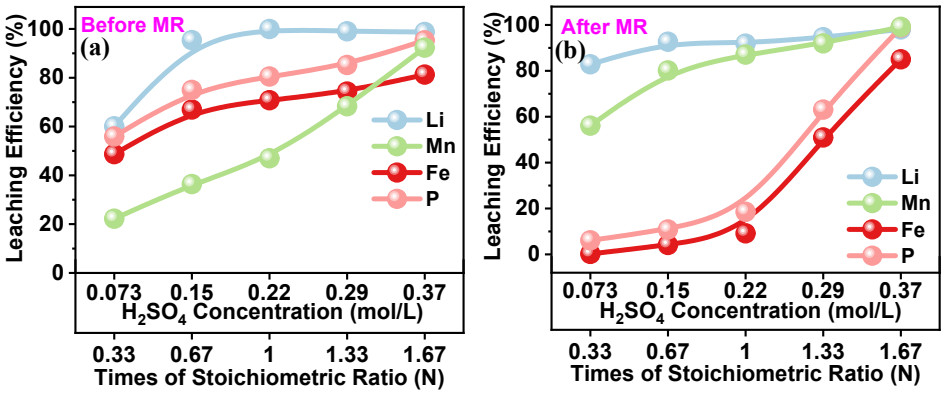

Fig. S8. Leaching behaviors for samples ($LiFePO_4$ and $LiMn_2O_4$) with different acid concentrations before (a) and after (b) mechanochemical reaction (conditions: molar ratio of LMO:LFP = 1:3, rotation speed- 650 rpm, mechanical milling time- 5 h, mass ratio of ball to powder- 50:1).

Table S1 A brief comparison of the traditional methods with mechanochemical method for the recycling of valuable metals from Spent LIBs [1-3]

Recycling method	Advantages	Disadvantages
Pyrometallurgy	Wide application; Large-scale; Less pretreatment.	Extensive energy consumption; Significant loss of Li; Harmful gases emission.
Hydrometallurgy	High efficiency; High purified products; Low energy consumption; Flexible recycling processes for different metals.	Complicated pretreatment; Extensive chemical consumption; Eeffluent discharging; Uneconomical for (LFP) batteries.
Mechanochemistry	Avoidance of extra wastes; Mild and safe processing environment; High reactivity derived by mechanochemical force.	Limited processing capacity; Long processing time; Additional further refining.

Table S2 Analytical methods.

No.	Instrument	Types	Area
1	Laser Particle Sizer	NAMO-ZS	Malvern, Britain
2	FT-IR spectroscopy	Scientific Nicolet iS10	Thermo Fisher, U.S.A.
3	Raman spectra	DXRxi	Thermo Fisher, U.S.A.
4	X-ray diffraction (XDR)	Dmax-RB12KW	Rigaku, Japan
5	Nitrogen gas adsorption instrument	ASAP 2460 sn:506	Micromeritics, U.S.A.
6	Contact angle meter (sessile drop method)	JY-82B Kruss DSA	Dataphysics Instrument Co., Ltd., Germany.
7	X-ray photoelectron spectroscopy (XPS)	AXIS SUPRA	Kratos, Britain
8	High-resolution field emission transmission electron microscopy (HRTEM)	JEM-2100F	JEOL, Japan
9	Inductively Coupled Plasma Optical Emission Spectrometer (ICP-OES)	Optima 5300 DV	Perkin Elmer Instruments, U.S.A.
10	Field Emission Scanning Electron Microscopy (FESEM)	MIRA3	TESCAN
11	X-ray EDS Analysis	X-MAX	Oxford, Britain

Table S3 Normal diffraction JCPDS cards of related compounds.

Compounds	Normal diffraction JCPDS cards
$LiCoO_2$	PDF#75-0532
Co_3O_4	PDF#43-1003
$LiFePO_4$	PDF#81-1173
$FePO_4$	PDF#29-0715

Table S4 Fitting peaks of XPS spectra for the Co2p of LCO powders activated after different milling times.

		Co $2p_{3/2}$				Co $2p_{1/2}$				Content (wt%)	
		Peak1 Co^{3+}	Peak2 Co^{2+}	Peak3 Co^{2+} Sat	Peak4 Co^{3+} Sat	Peak5 Co^{3+}	Peak6 Co^{2+}	Peak7 Co^{2+} Sat	Peak8 Co^{3+} Sat	Co^{2+}	Co^{3+}
0	Position(eV)	779.65	780.85	781.47	789.45	794.65	795.85	797.24	805.00	29.54	70.46
	Aera (%)	22.69	9.51	19.58	8.61	11.34	4.76	12.59	10.91		
1h	Position(eV)	779.82	781.04	783.47	789.80	794.91	796.24	798.00	804.34	53.25	46.75
	Aera (%)	11.04	12.57	28.55	13.03	5.52	6.29	9.01	13.98		
3h	Position(eV)	779.70	780.95	782.57	787.88	794.80	796.15	798.89	804.44	60.73	39.27
	Aera (%)	9.52	14.24	21.41	22.06	4.29	7.12	8.73	12.63		
5h	Position(eV)	779.67	780.81	783.24	788.12	794.66	796.01	797.77	803.06	72.69	27.31
	Aera (%)	5.90	16.43	26.06	20.96	2.95	7.12	5.98	14.59		
7h	Position(eV)	779.62	780.57	783.25	788.36	794.62	795.87	798.71	804.48	73.36	26.64
	Aera (%)	6.16	16.97	24.10	15.02	3.08	8.48	11.76	14.42		
9h	Position(eV)	779.91	781.11	783.94	788.89	795.01	796.61	799.00	803.60	73.45	26.55
	Aera (%)	6.47	17.65	24.02	15.13	3.04	8.65	7.42	17.62		

The fitting data of the Co2p XPS spectra was calculated by the XPS peak software (Casa XPS).

Content of Co^{2+}= ($Aera_{peak2}$ +$Aera_{peak6}$)/(($Aera_{peak1}$ +$Aera_{peak2}$ +$Aera_{peak5}$ +$Aera_{peak6}$)

Content of Co^{3+}=($Aera_{peak1}$ +$Aera_{peak5}$)/(($Aera_{peak1}$ +$Aera_{peak2}$ +$Aera_{peak5}$ +$Aera_{peak6}$)

Table S5 Fitting peaks of XPS spectra for the Fe2p of LFP powders activated after different milling times.

		Fe $2p_{3/2}$				Fe $2p_{1/2}$				Content (wt%)	
		Peak1 Fe^{2+}	Peak2 Fe^{3+}	Peak3 Fe^{2+} Sat	Peak4 Fe^{3+} Sat	Peak5 Fe^{2+}	Peak6 Fe^{3+}	Peak7 Fe^{2+} Sat	Peak8 Fe^{3+} Sat	Fe^{2+}	Fe^{3+}
0	Position(eV)	710.44	712.20	714.15	718.10	724.04	725.80	728.32	731.88	76.26	23.74
	Aera (%)	21.60	7.91	29.93	6.59	10.36	5.29	14.37	3.95		
1h	Position(eV)	710.47	711.93	713.96	716.9	723.87	725.33	726.68	730.60	52.65	47.35
	Aera (%)	12.97	11.91	15.19	24.16	6.48	5.58	7.31	16.41		
3h	Position(eV)	710.45	712.50	714.57	718.02	723.88	725.99	728.00	731.82	42.01	57.99
	Aera (%)	12.42	17.48	9.83	23.59	6.83	9.09	4.59	16.18		
5h	Position(eV)	710.49	712.06	714.60	719.04	723.79	725.36	727.37	731.01	33.86	66.14
	Aera (%)	8.16	16.27	19.59	24.48	4.08	7.64	8.53	11.25		
7h	Position(eV)	710.49	712.14	714.63	718.69	723.86	725.59	727.40	731.89	31.15	68.85
	Aera (%)	9.13	21.71	14.65	21.20	5.11	9.77	7.73	10.71		
9h	Position(eV)	710.39	711.92	714.38	718.64	723.89	725.42	727.17	731.93	31.31	68.69
	Aera (%)	8.56	18.78	18.35	19.19	4.28	9.39	8.74	12.70		

The fitting data of the Fe2p XPS spectra was calculated by the XPS peak software (Casa XPS).

Content of Fe^{2+}= $(Aera_{peak1} + Aera_{peak5})/((Aera_{peak1} + Aera_{peak2} + Aera_{peak5} + Aera_{peak6})$

Content of Fe^{3+}=$(Aera_{peak2} + Aera_{peak6})/((Aera_{peak1} + Aera_{peak2} + Aera_{peak5} + Aera_{peak6})$

Table S6 Thermodynamic data for the related species at 298.15 K.

Substance	$\Delta_f G_m^\theta$ (kJ/mol)	Ref.	Substance	$\Delta_f G_m^\theta$(kJ/mol)	Ref.
$LiFePO_4$	-1480.97	[4]	$LiCoPO_4$	-5660.10	[5]
$LiCoO_2$	-620.22	[6]	$LiNi_{0.5}Co_{0.2}Mn_{0.3}O_2$	-640.04	[7]
CoO	-214.00	[8]	$LiMn_2O_4$	-1374.80	[9]
Li_2O	-561.20	[8]	H_2SO_4	-689.90	[8]
Co_3O_4	-774.00	[8]	$CoSO_4$	-782.40	[8]
Li_3PO_4	-2127.45	HSC 6.0	Li_2SO_4	-1331.20	[8]
Fe_2O_3	-742.20	[8]	$NiSO_4$	-790.30	[8]
$FePO_4$	-1179.30	[4]	$MnSO_4$	-972.80	[8]
FeO	-251.40	[8]	H_2O	-237.14	[8]

Table S7 Gibbs free energy values ($\Delta_r G_m$) for Eq. (4)-(13) at 298.15 K.

No.	Reaction equation	$\Delta_r G_m$ (kJ/mol)
(4)	$10LiFePO_4+10LiNi_{0.5}Co_{0.2}Mn_{0.3}O_2+20H_2SO_4=10FePO_4+2CoSO_4+10Li_2SO_4+5NiSO_4+3MnSO_4+20H_2O$	-3273.4
(5)	$3LiFePO_4+LiMn_2O_4+4H_2SO_4=3FePO_4+2MnSO_4+2Li_2SO_4+4H_2O$	-517.155
(6)	$LiFePO_4+LiCoO_2=FePO_4+CoO+Li_2O$	146.69
(7)	$LiFePO_4+3LiCoO_2=FePO_4+Co_3O_4+2Li_2O$	265.93
(8)	$2LiFePO_4+Co_3O_4=2FePO_4+3CoO+Li_2O$	174.14
(9)	$3LiFePO_4+3LiCoO_2=2Li_3PO_4+FePO_4+3CoO+Fe_2O_3$	-514.83
(10)	$2LiFePO_4+4LiCoO_2=2Li_3PO_4+Co_3O_4+CoO+Fe_2O_3$	-1782.72
(11)	$3LiFePO_4+6LiCoO_2=3Li_3PO_4+2Co_3O_4+Fe_3O_4$	-208.32
(12)	$3LiFePO_4+Co_3O_4=Li_3PO_4+3CoO+2FePO_4+FeO$	-162.54
(13)	$2LiFePO_4+2LiCoO_2=2LiCoPO_4+Fe_2O_3+Li_2O$	-8421.22

Notes: It is worth to notice that the values of $\Delta_r G_m$ for Eq. (6)-(8) are positive, indicating that these chemical reactions cannot be spontaneously processed under such available conditions. However, it has been well acknowledged that high temperature and high pressure can be generated during the intense collision among the fine particles with balls, which can promote and realize the chemical reactions that are thermodynamic impossible[10, 11]. Besides, it has been proved by this study from the experimental, characterization and theoretical results that the targeted products have been generated by the mechanochemical process.

Reference:

1. F. Arshad, L. Li, K. Amin, E. Fan, N. Manurkar, A. Ahmad, J. Yang, F. Wu and R. Chen, *ACS Sustain. Chem. Eng.* , 2020, **8**, 13527-13554.
2. J. J. Roy, S. Rarotra, V. Krikstolaityte, Z. K. W, Y. D. Cindy, X. Y. Tan, M. Carboni, D. Meyer, Q. Yan and M. Srinivasan, *Adv. Mater.*, 2021, DOI: 10.1002/adma.202103346, 2103346.
3. X. Xia and P. Li, *Sci. Total Environ.*, 2022, **814**, 152870.
4. A. V. Churikov, A. V. Ivanishchev, A. V. Ushakov, I. M. Gamayunova and I. A. Leenson, *Journal of Chemical & Engineering Data*, 2013, **58**, 1747-1759.
5. S. L. Shang, Y. Wang, Z. G. Mei, X. D. Hui and Z. K. Liu, *J. Mater. Chem.*, 2012, **22**, 1142-1149.
6. S. Wang, C. Wang, F. Lai, F. Yan and Z. Zhang, *Waste Manage. (Oxford)*, 2020, **102**, 122-130.
7. Y. Lixin, Master of Engineering Lanzhou University of Technology 2019.
8. J. A. Dean, *Langes handbook of chemistry*, R. R. Donnelley & Sons Company, New York 1999.
9. Z. Li, L. He, Z. w. Zhao, D. Wang and W. Xu, *ACS Sustainable Chemistry & Engineering*, 2019, **7**, 16738-16746.
10. Q. Wu, Mechanochemistry of inorganic materials, Chemical Industry Press, Beijing, 2008.
11. H. Yang, Mechanochemistry of materials, Science Press, Beijing, 2009.